Daytime Passive Radiative Cooling by Ultra Emissive Bio-inspired Polymeric Surface

S.Y. Jeong [1], C.Y. Tso [1,], Y.M. Wong [2], C.Y.H. Chao [3], B. Huang[2]*

[1] School of Energy and Environment, City University of Hong Kong, Tat Chee Avenue, Kowloon, Hong Kong, China

[2] Department of Mechanical and Aerospace Engineering, The Hong Kong University of Science and Technology (HKUST), Hong Kong, China

[3] Department of Mechanical Engineering, The University of Hong Kong, Hong Kong, China

* Corresponding Author Tel.: +852 3442 4623

E-mail address: chiytso@cityu.edu.hk

Address: School of Energy and Environment, City University of Hong Kong, Tat Chee Avenue, Kowloon, Hong Kong, China

Abstract

Saharan silver ants can maintain their body temperature below ambient air due to unique triangular shaped hairs that enhance solar reflection and thermal emission through a transparent window that lies in the atmosphere. Applying this thermoregulatory prismatic structure to polydimethylsiloxane (PDMS), highly emissive in the 8-13 μm spectrum, we present a geometrically modified polymer-based daytime passive radiative cooler. The selective thermal emitter was fabricated based on the optimized prismatic structure from Finite Difference Time Domain (FDTD) simulations. The average emissivity within the 8-13 μm spectrum was enhanced to 0.98 by the gradient refractive index effect, while the average solar reflectivity in the visible and near-infrared spectrum was measured to be 0.95. The net radiative cooling power is estimated to reach 144 W/m^2, exceeding records of previously reported radiative coolers. Last, in Hong Kong's hot and humid climate, a field test successfully demonstrated cooling by 6.2 °C below the temperature of ambient air corresponding to a net cooling power of 19.7 W/m^2 in a non-vacuum setup during the peak daytime with shading. This is the largest temperature reduction observed in a tropical region for daytime passive radiative cooling. Our work presents an alternative method to enhance passive thermal emission and may facilitate its world wide application in eco-friendly space cooling.

Keywords: Gradient refractive index, Mie-scattering, Radiative cooling, Saharan silver ant, Selective emission, Thermal radiation

1. Introduction

Daytime passive radiative cooling proposes a new eco-friendly strategy to solve the high energy demand for building space cooling. Conventional and widely used cooling methods require

external power sources or devices where high energy consumption is inevitable due to the necessities of everyday life. In contrast to the cooling methods utilizing resources and energy, passive radiative cooling solely focuses on the natural cooling strategies of near perfect solar energy reflection which lies in the visible (VIS) and near-infrared (NIR) spectrum, minimizing thermal absorption of incident solar irradiation. Furthermore, in the mid-infrared (MIR) spectrum (8-13 μm), the strong selective thermal radiation occurs from an object efficiently delivering thermal energy to the cold heat sink of outer space (~ 3 K) through the atmospheric transparency window where radiation absorption is very low in the 8-13 μm spectrum. Nocturnal passive radiative cooling has been successfully conducted [1–10]; however, high cooling demands occur at peak hours during the daytime.

Recently, scientists and engineers have demonstrated a sky facing surface able to sustain its temperature below the temperature of ambient during daytime with a passive selective radiation strategy. A typical configuration of a daytime passive radiative cooler can be elaborated as two layered structures, including the top emissive layer and bottom reflective layer. Various materials and geometrical modifications in the top emissive layer were investigated to produce a cooling effect during daytime, such as photonic, plasmonic, biomimetic materials, etc. A photonic radiative cooler with a thermal emitter composed of seven repetitive layers of hafnium oxide (HfO_2) and silicon dioxide (SiO_2) and a solar reflector of silver (Ag), demonstrated a radiated power of 40 W/m^2 and a daytime cooling performance of nearly 5 °C reduction below the temperature of ambient air [11]. This nanophotonic device which showed promising cooling performance in a dry region was tested in the sub-tropical climate of Hong Kong [12, 13]. A temperature reduction of 6-7 °C was achieved under a clear night sky, but daytime cooling was not achieved in the humid

climate since the mid-infrared thermal emission is weakened by the huge amount of atmospheric water vapor. The nano-photonic approach requires precise and accurate fabrication, thus, the simplified radiative cooler was developed by deposition of silicon nitride (Si_3N_4), and amorphous silicon (Si) on the top of a solar reflector of aluminum (Al) and in a vacuum condition, a strong daytime radiative cooling was achieved by 42 °C reduction below the ambient in the dry climate of California, USA [14]. A polymer based simplified passive cooler was proposed, designed with a polydimethylsiloxane (PDMS) polymer on top of the silver (Ag) sputtered glass (SiO_2) wafer achieving a daytime cooling of 8.2 °C below the ambient relevant to a high radiative power of 127 W/m^2 in low humidity California [15]. Photonic crystal structures theoretically and experimentally demonstrated selective thermal emission by surface plasmonic resonance [16–29]. Different types of plasmonic radiative coolers were proposed including micropillar patterns on Al plate [30] and Ag deposited micro-patterned silicon (Si) wafers [31] demonstrating a numerically analyzed net cooling power of 100 W/m^2. Generally, literatures report on lab scale radiative coolers with limited practical applications. Comprehensive reviews on a scaled-up glass-polymer hybrid radiative cooler by reel-to-reel processing has been carried out [32, 33]. Motivated by a polymeric radiative cooler with silicon carbide (SiC) and dispersed SiO_2 micro-particles [34], a scalable SiO_2 micro-particle doped polymeric radiative cooler with the optimized particle size enhancing selective thermal emission in mid-infrared (MIR) emission was manufactured, recording a radiative power of 93 W/m^2 [33]. Daytime passive radiative coolers can be directly attached to fabrics [35, 36] and electronics [37, 38] for efficient cooling, or they can be integrated in a refrigeration cycle of HVAC systems in buildings as a condenser which saves energy consumed in space cooling due to its cooling performance without energy input [39-41].

Both organic and inorganic materials with strong emission property in the MIR wavelength spectrum (8-13 μm) were used as the base thermal emission substrate for passive radiative cooling [11–34]. In this study, for the first time, photonic approach on polymer was utilized to design a passive radiative cooler where geometry modification in polymer has been seldom considered to further enhance emission properties due to the challenge of controlling defects. However, polymer is a very attractive material due to its low cost, compatibility with various patterns, offering the required optical, electronic, and mechanical properties required [34, 42]. This work has been triggered by the Saharan silver ant shown in Fig. 1a that possesses two different passive thermal regulatory effects and successfully survives in extremely hot deserts. The Saharan silver ant has unique shaped hairs, in the form of triangular prisms, providing two thermoregulatory effects as shown in Fig. 1b that allows the ant to keep cool under the extremely strong sunlight of the Saharan desert [43–45]. The triangular shaped hair induces enhancement in total internal reflection within the solar spectrum (0.25 – 2.5 μm) resulting in high reflection of incident solar irradiance. The enhancement is realized by Mie scattering which takes place in situations where the size of the object is comparable to the wavelength of incident light, and for the ant, the scattering effect occurs at ~2 μm [46]. Furthermore, enhanced MIR emissivity of the hair facilitates heat dissipation of thermal energy accumulated in the ant's body which can easily escape through the transparent window. Shi et al. reported that due to its strong enhancement in solar reflection, the hair structure can be applied to develop a radiative cooler with a high reflective surface which does not require a metal reflector. However, the triangular prismatic structures were only able to achieve solar reflection of ~60 % which is far from the solar reflection requirement for radiative coolers (i.e. > 95 %) [44], thus, the application approach was newly established to enhance MIR thermal radiation of the daytime radiative cooling by utilizing gradual refractive index change effective in 8-13 μm.

In this study, we propose a selective thermal emission device with application of the unique triangular prism shape of the Sahara silver ants' hair to perform enhanced radiative cooling performance. First, we investigated improvement in MIR thermal emission utilizing the micro-scale triangular prism structure compared to a conventional flat, multi-layered film and hair resembling a circular tube-structured cooler. The following study was conducted on the triangular structure for optimization to achieve the strongest thermal emission by controlling parameters such as the geometrical configurations and size. After computational optimization of the triangular structure, a passive radiative cooler employing the triangular prism array was then manufactured by a microfabrication process. To verify the result of the simulation study, the optical characteristic of the fabricated cooler was measured and a comparative study with the uniformly layered cooler was conducted. Based on the measured optical properties, its cooling performance was analyzed numerically with energy balance equations. Lastly, to test its practicality under the humid weather condition of Hong Kong with a low transparent atmospheric window, field investigations were carried out and the cooling performance was observed. This study indicates geometrical modification as a potential solution to improve selective thermal emission besides the selection of various materials, which can significantly improve the passive radiative cooling effect by scaling down, reducing materials required for manufacturing but enhancing the cooling power. This indicates that the biomimetic radiative cooler could be an attractive non-energy-consuming solution to reduce air conditioning costs for buildings in the near future.

2. Material and methods

2.1. Design and optimization method

In this study, we propose the bio-inspired passive daytime radiative cooler with a design of a top MIR emissive layer of PDMS and SiO_2 that strongly radiates in the 8-13 μm spectrum and a bottom solar reflective layer composed of Ag which can provide solar reflection above 95 %. Optimization was mainly focused on achieving the highest emissivity within the targeted MIR range (8-13 μm) due to the major contribution in net radiative cooling performance. PDMS and SiO_2 are already well known for being selectively emissive in 8-13 μm wavelength range due to a high value of imaginary permittivity [47]. Furthermore, the proposed cooler possesses an advantage of easy fabrication due to widely available SiO_2 substrate wafer (400-500 μm) and flexible material property of PDMS which can be easily shape to desired geometries on the surface by a nano-imprinting process. The great freedom to shape PDMS allows us to study the improvement of optical properties especially emissivity in different configurations. The geometrical structure on the surface of the PDMS emitter was optimized by utilizing FDTD simulations considering different geometries and sizes. After optimization, a comparison study regarding MIR emission between our optimized bio-inspired cooler and conventional flat surface cooler was performed. Prior to the fabrication and field experiment, FDTD optical computational analysis which directly solves Maxwell equations was utilized to achieve the highest net cooling power by optimizing geometrical structures of the PDMS emitter surface and the overall design of the cooler.

2.2. Fabrication

For the microfabrication of the optimized bio-inspired daytime radiative cooler, a mold with triangular prism patterns needs to be fabricated first which can later be used to print patterns on the PDMS layer. A 525 μm thick P-type 4" silicon wafer was used as the substrate for the triangular prism array mold. The silicon wafer first underwent pre-photolithography cleaning in Piranha

154 solution, mixture of 10:1 (v/v) H_2SO_4:H_2O_2, at 120 °C for 10 mins to remove organic residues and
155 gross contaminants. Native oxide layer on the silicon wafer surface was removed by hydrofluoric
156 acid solution, mixture of 1:50 (v/v) HF:H_2O, for 1 min. After the cleaning process, a thin silicone
157 oxide layer of 60 nm was produced on the silicon wafer surface by thermal oxidation using a
158 diffusion furnace at a temperature between 800 - 1200 °C. The purpose of the silicon oxide layer
159 is to protect the unexposed silicon area during an etching process. Triangular prism arrays were
160 photo-lithographically patterned on a 1-um-thick layer of photoresist (PR), HPR 504, on top of the
161 silicon dioxide layer. The pattern consists of repetitive rectangular lines with a uniform width and
162 a gap of 1.5 μm between each line. Patterns for different line widths were considered in fabrication
163 varying from 8-13 μm to study the cooling performance of different triangular sizes. The silicon
164 dioxide layer was etched using an advanced oxide etching (AOE) process that etches only the
165 exposed photoresist layer until the silicon surface is exposed. The photoresist layer was solely
166 required for leaving the pattern on the silicon dioxide layer and therefore, after etching of the
167 silicon dioxide layer, it was completely stripped by O_2 plasma treatment. Before the silicon etching
168 process started, the silicon wafer was treated with hydrofluoric acid again for complete removal
169 of native oxide on the exposed silicon surface which might hinder the process of silicon etching.
170 The silicon wafer was then immersed into a tetramethylammonium hydroxide (TMAH) solution
171 (25 wt. %), a silicon etchant, at temperature of 90 °C and only the unprotected silicon area was
172 etched. TMAH etches silicon leaving V-grooves and the angle between the sidewalls and the (100)
173 plane is 54.7 °. Anisotropic etching property of TMAH achieves triangular prism arrays on the
174 silicon wafer. Typical etch rate of TMAH for the (100) plane was 1.0 μm/min and for the (110)
175 plane was 1.4 μm/min at 90 °C [48]. The etching time was carefully controlled based on the widely
176 known etching rate of silicon. Silicon dioxide layer was perfectly removed by buffered oxide etch

(BOE) solution, mixture of 6:1 (v/v) NH_4F:HF, and the mold for the triangular prism array structure was completed. Totally, three molds for different triangular size parameter of 8, 9, and 10 μm were fabricated. The patterned surface of the silicon mold was sputtered with 320 nm of chromium which acts as a PDMS anti-adhesion layer. PDMS and its curing agent were mixed together in the mass ratio of 10:1 then spin-coated with 20 μm thickness on a 525 μm thick 4 cm x 4 cm glass substrate with 160 nm thick silver sputtered at the back. On top of the spin-coated PDMS, the silicon mold facing patterned surface toward PDMS was pressed gently and cured in an oven at 80 °C for 4 hrs. After the curing process finished, the patterned silicon mold was gently removed, achieving a three layered passive radiative cooler sample consisting of a triangular prism array structured PDMS, glass and silver at the bottom. The fabrication process is elaborated more in Fig. S1 in the Supplementary Materials.

3. Theory/calculation

To carry out the cooling performance analysis numerically for the fabricated bio-inspired cooler such as the net cooling power and achieved temperature reduction below the temperature of ambient air, the energy balance state of the daytime passive radiative cooling was carefully investigated. The net radiative cooling power, P_{cool}, is shown below [11]:

$$P_{cool} = P_{rad}(T_{prc}) - P_{atm}(T_{atm}) - P_{sun} - P_{con}(T_{prc}, T_{atm}), \quad (1)$$

where P_{rad} is the thermally radiated power of the cooling device [W], T_{prc} is the surface temperature of the cooler [K], P_{atm} is the power absorbed by the passive radiative cooler from the ambient atmosphere [W], T_{atm} is the ambient atmosphere temperature [K], P_{sun} is the absorbed

power by the surface of the cooler from the incident solar irradiance [W], and P_{con} is the convective and conductive power gained by the cooler surface [W]. The radiative thermal energy emitted from the cooler at the cooler temperature, T_{prc}, is given by:

$$P_{rad}(T_{prc}) = A_{prc} \int d\Omega \cos\theta \int_0^{\infty} d\lambda I_{BB}(T_{prc}, \lambda)\varepsilon(\lambda), \quad (2)$$

where A_{prc} is the area of the sky facing cooler [m^2]. $I_{BB}(T,\lambda) = \frac{2hc^2}{\lambda^5}\frac{1}{e^{hc/(\lambda k_B T)}-1}$ is the spectral distribution of the thermal energy radiated by a black-body [$W/(m^3 sr)$] at any temperature T and h is Planck's constant of 6.63×10^{-34} J·s, c is the universal physical constant for speed of light which is 3.00×10^{8} m/s, λ is wavelength [m], and k_B is denoted as the Boltzmann constant of 1.38×10^{-23} J/K, $\varepsilon(\lambda)$ refers to the emissivity spectra (0.25- 25 μm) of the radiative cooling devices and the measured emission spectrum of the coolers used. $P_{atm}(T_{atm})$ is the absorbed power by the cooler surface from the thermal radiation emitted from the surrounding atmosphere at the temperature of T_{atm} and can be defined as:

$$P_{atm}(T_{atm}) = A_{prc} \int d\Omega \cos\theta \int_0^{\infty} d\lambda I_{BB}(T_{atm}, \lambda)\varepsilon(\lambda)\varepsilon_{atm}(\lambda), \quad (3)$$

where $\varepsilon_{atm}(\lambda)$ is the emission spectrum (0.25-25 μm) of the atmosphere [49]. Validation of the numerical model was carried out by comparing the numerically estimated cooling power with previous studies [11–15, 33] by using the widely known atmospheric transmittance data measured in Mauna Kea located in Hawaii, U.S.A. with conditions of 1.5 air mass and precipitable water vapor of 1.0 mm [50]. Thermal energy is emitted from the surrounding atmosphere and absorbed by the radiative cooler with the ratio of its emissivity degrading net cooling performance. The law

of Kirchhoff's radiation clearly states that the material's absorptivity and emissivity can be considered equal because under a thermodynamic equilibrium state, the fraction of an emissive power from a perfect black-body shows it to be equivalent to its ratio of the incoming power to the absorbed power of the object [2–10].

$$P_{sun} = A_{prc} \int_0^{\infty} d\lambda I_{AM1.5}(\lambda)\varepsilon(\lambda), \quad (4)$$

is the absorbed power by the radiative cooler from incoming solar irradiance. $I_{AM1.5}$ is the AM 1.5 G spectrum which can be defined by the solar intensity of densly populated regions which are located at moderate altitude [51] and used widely in the photovoltaic industry [52]. P_{con} is the parasitic heat delivered to the cooler from the surrounding atmosphere by conduction and convection and can be defined as:

$$P_{con}(T_{prc}, T_{atm}) = A_{prc} h_{con}(T_{atm} - T_{prc}), \quad (5)$$

where h_{con} is the heat transfer coefficient for the heat transfer between the cooler and the surrounding atmosphere due to conduction and convection [W/(m^{2}K)].

4. Results and Discussion

4.1. FDTD optimizations

The emission spectra were investigated for three different geometrical configurations of the PDMS thermal emitter with various characteristic lengths of the proposed geometries. These configurations are conventional uniform flat surfaces, ordinary hair resembling periodic circular

arrays, and lastly, Saharan silver ant hair inspired periodic triangular arrays. The optical property comparison in different geometrical structures is to show that the triangular prism shape adopted surface can enhance MIR emissivity of the conventional flat emitter. The PDMS emitter with circular arrays which represents commonly recognized hair was also studied to further investigate the uniqueness of the triangular hair structure compared to the ordinary hair structure. Referring to Fig. 1c, characteristic lengths (a) of the geometries were selected as the thickness of the uniform flat surface, the diameter of the circle, and the bottom length of the triangle. The triangular structure was set to isosceles triangle with equal angle of 54.7° because the angle is limited to that for the wet etching process on a silicon wafer. Knowing that Mie scattering occurs when incoming wavelength and object share similar size, characteristic lengths of the proposed structure were selected within the range of 2-15 μm to investigate MIR emissivity enhancement of the emitter caused by the scattering effect. Fig. 1c shows the averaged MIR emissivity of three different geometries along the characteristic lengths. This plot represents the PDMS emitter with triangular arrays on the surface, always achieving a stronger thermal emission property than the other two geometrical configurations. Furthermore, when the size parameter of the triangle was between 8-13μm, the simulated average emissivity within the atmospheric transparent window showed a higher value than when the size was outside this range. This is mainly due to the triangular prism structure with a size between 8-13 μm that can provide a gradual change in the refractive index in 8-13 μm between air and PDMS. Impedance mismatch occurring between air and PDMS can be reduced, enhancing the overall emissivity of PDMS. Different size of triangular prism PDMS gradient index layer within the size parameter of 8-13 μm shows varying influence on emissivity within this bandwidth due to the difference in resonance points. The size parameter of 8 μm which is four times larger than the original hair showed the strongest improvement in thermal emission

within 8-13 μm, resulting in an average emissivity value of 0.98. Fig. 1d shows the emission spectra for three different configurations sharing the same characteristic length of 8 μm in the wavelength range of 8-13 μm. At the same characteristic length, the triangular PDMS emitter clearly shows the highest MIR emissivity over the other two emitters. Referring to the FDTD simulation study, triangular structure is the best for enhancing thermal emission within MIR and the triangle with optimized characteristic length of 8 μm induces the most Mie scattering within 8-13 μm, resulting in the highest average emissivity of 0.98 within 8-13 μm.

4.2. Optical measurement and numerical analysis

Based on the simulation study, a PDMS-SiO_2-Ag three layered cooler, in which the PDMS thermal emitter (4-inch wafer) shown in Fig. 2a was of an optimized triangular geometry with a characteristic length of 8 μm, was micro-fabricated. Silicon molds with triangular arrays shown in Fig. 2b were used to print patterns on the PDMS surface. Fig. 2c shows the enlarged cross-section of the silicon mold. Validation of the simulation results was followed by investigating PDMS emitters with different characteristic lengths of the triangle, 8 μm, 9 μm and 10 μm, together with a uniform 100 μm thick PDMS emitter. To investigate the overall cooling performance improvement of the bio-inspired cooler compared to the previously proposed radiative coolers [15], the uniform 100 um thick PDMS emitter was chosen rather than a uniform PDMS emitter with a similar characteristic length of triangular patterned PDMS emitter. To compare and understand the optical properties of the samples, the emissivity of the samples over the ultraviolet (UV) to IR wavelength ranges shown in Fig. 3a were measured by an UV/VIS/NIR spectrometer and Fourier transform infrared spectroscopy (FTIR). Fig. 3b shows the emissivity spectrum in the UV to NIR region of the coolers with PDMS in uniform and triangular structures with size

parameters at 8, 9, and 10 μm. Solar radiation absorbed by the coolers can be numerically calculated by the multiplication of the measured absorptivity of coolers within UV-NIR and AM 1.5 G solar irradiance at unit wavelength. All four different samples of radiative coolers showed low solar absorption power density about 20-25 W/m^2 that mainly absorbed within the ultraviolet spectrum. The triangular prism structure did not show any improvement in solar reflection but mainly enhanced the thermal radiation of the passive radiative cooler. Fig. 3c shows the emissivity spectra of the four different coolers in the wavelength range of 8–13 μm. The average emissivity for the uniform PDMS cooler was 0.92 and the triangular PDMS cooler with a size parameter of 8 μm showed 0.98, an enhancement of 6.5%. The triangular PDMS cooler with a size parameter of 10 μm showed the lowest emissivity (0.93) among the patterned PDMS coolers, indicating the triangular structure to have better emission performance within the 8-13 μm spectrum range than the uniform PDMS cooler. Lastly, a comparison solar reflectivity and MIR emission spectrum of the previously reported daytime passive radiative coolers [11, 13-15, 53, 54] with the triangular patterned PDMS cooler was conducted to understand the performance improvement. Fig. 4a shows that the bio-inspired triangular PDMS cooler is not really outstanding in solar reflectance among all the radiative coolers previously studied. Due to the wide usage of silver as a reflector in the daytime passive radiative coolers, most coolers including the bio-inspired triangular PDMS cooler (i.e. this work) show high solar reflection (i.e. at least 97%). The highest solar reflection was achieved by the PTFE-Ag cooler which can reflect 99% of incoming solar irradiance, absorbing only ~10 W/m^2, which is 15 W/m^2 less than the bio-inspired triangular PDMS cooler (i.e. this study) [53]. However, Fig. 4b shows that the bio-inspired triangular PDMS cooler shows very clear difference in MIR emissivity by having almost unity spectrum in the 8-13 um wavelength. This obvious distinction shows the developed radiative cooler has almost achieved the maximum

emission performance for the daytime passive radiative cooling technique. The prismatic structure obviously showed superiority in MIR emissivity compared to the uniform surface and with the measured optical characteristics, the cooling performance improvement can be investigated numerically.

To validate the result analyzed by the energy balance equation, the cooling performance of a fabricated uniform 100 µm thick PDMS silica-mirror was analyzed based on its measured optical properties and compared with the previously reported value [15]. When there are no parasitic heat gains from the ambient atmosphere (i.e. h_{con} = 0 W/(m^{2}K)), Fig. 5a shows that the fabricated uniform 100 µm PDMS cooler can passively provide a net cooling power of 127 W/m^2 at the temperature of the surrounding atmosphere, T_{atm}, of 27 °C that perfectly matches with the previously reported net cooling power of the uniform 100 µm thick PDMS silica-mirror [15]. The patterned PDMS cooler can provide the maximum net cooling power of 144 W/m^2 at the ambient air temperature of 27 °C which corresponds to an enhancement of 13.4 % compared to uniform PDMS cooler. The ideal passive radiative emitter, perfect solar reflection in the spectrum of 0.3 – 2.5 µm and perfect emission in the spectrum of 8 -13 µm, was estimated to provide a maximum net radiative cooling power of 132 W/m^2 at the ambient air temperature of 27 °C [55]. However, the cooling performance can be further enhanced by exploiting spectrum regions outside the atmospheric transparent window, 2.5 – 8 µm and 13 – 25 µm. Utilizing this broad spectrum region, 2.5 - 25 µm, an ideal radiative cooler with perfect solar reflection in the spectrum of 0.3 - 2.5 µm and perfect emission in the spectrum of 2.5 - 25 µm can produce 207 W/m^2 maximum cooling power at the ambient of 27 °C [55]. The total thermal radiation absorbed from the atmosphere to the cooler is increased but the outgoing thermal emission from the cooler exceeds the incoming

radiation, thereby enhancing the net cooling performance. The triangular structure greatly enhances emissivity within 8 - 13 μm and outside the main atmospheric transparent window, ultimately exceeding the cooling power of the narrow-band ideal radiative cooler. Fig. 5b presents an estimated cooling power of the cooler at a condition where the ambient, T_{atm}, is 27 °C and a parasitic heat coefficient of h_{con}= 10 W/(m^{2}K) [15]. In Fig. 5b, temperature of the cooler is reduced below the ambient air temperature by 8.7 °C for the uniform 100 μm PDMS cooler. The patterned PDMS cooler can decrease the surface temperature by a maximum of 9.8 °C which shows the triangular structure greatly enhances the cooling performance compared to the uniform PDMS cooler.

4.3. Field investigation

To validate the numerically estimated cooling performance and study the actual cooling behavior in non-ideal atmospheric conditions, 24-hour field investigations were conducted under the sky condition of Hong Kong. The radiative cooling performance investigation was performed on the building roof top where the cooler can perfectly face the sky. In the experiment setup, minimizing the parasitic heat gains to the coolers was the top priority in order to maximize the net cooling power. The experiment site was perfectly covered by a calcium-magnesium silicate thermal insulation sheet to minimize the conductive heat generated from the concrete surface heated from the sunlight. Petri dishes with three acrylic legs which can minimize the contact surface with the ground were placed on top of the sheet. The fabricated coolers were placed in the Petri dishes to limit the thermal contact with the ambient air. Additional acrylic supporting structures were also fabricated to minimize the contact with the Petri dishes. Finally, to minimize the convective heat transfer by wind, the Petri dishes were covered by a very thin polyethylene film which is

transparent within the wavelength ranges of solar radiation and passive radiative cooling. A detailed schematic design of the experimental setup can be found in Fig. 6a. Fig. 6b shows the experimental setup on the rooftop of a building. A data acquisition device, National Instruments NI 9213, was used to record (frequency: 1 s, accuracy: ±0.02 °C) the temperatures of coolers and ambient air measured by thermocouples. Thermocouples used in the field investigations were calibrated to eliminate measurement error and directly attached to the back side of the cooler having the silver layer. The experiment was conducted during clear days of June and September.

Totally, 2 different samples were prepared to carry out the comparative study. These consisted of a uniform 100 µm PDMS-SiO_2-Ag cooler and an 8 µm triangular patterned PDMS-SiO_2-Ag cooler that showed the highest net cooling power among all the patterned coolers with different sizes of triangle. Fig. 7a presents the four different temperature profiles of the 8 µm triangular and the 100 µm thick uniform PDMS-SiO_2-Ag coolers with and without solar shade for a 48 hr cycle measurement in Hong Kong (Date: Sep-30-2018 to Sep-31-2018). The average relative humidity of these two days was 87 % and the sky was very clear with 0-1 oktas. Under the humid Hong Kong weather, no matter shaded or unshaded, during the night time, both the triangular patterned and the uniform cooler showed cooling effects with a temperature reduction of 6.1 °C and 5.2 °C below the ambient air temperature, respectively. The triangular patterned PDMS cooler showed a lower surface temperature by average 1 °C than the uniform PDMS cooler. The uniform PDMS cooler was reported to have a temperature decrease of 8.4 °C during night time of Pasadena, California [15]. The lower value of the measured temperature reduction below the ambient during the night time is due to the high relative humidity in Hong Kong. The transparency of the atmospheric window that lies in 8-13 µm spectrum is closely affected by the vapor concentration

384 in the atmosphere that results in low transparency, i.e., high absorption of atmosphere is due to the
385 high relative humidity and this limits the escape of the thermal radiation to the cold universe. The
386 MIR absorption of atmosphere enhanced by three-folds as the precipitable water vapor increases
387 from 1.5 cm to 6 cm [3], showing the limitation of the passive radiative cooling in humid weather.
388 Conditions of low humidity and cloudless sky can result in strong transmittance in the MIR
389 spectrum facilitating the radiative cooler to produce the ideal cooling performance. However, the
390 field investigation showed that the triangular pattern could enhance the radiative cooling effect,
391 reducing the temperature nearly 1 °C more than the uniform PDMS cooler. Fig. 7b (i.e. a zoom-in
392 figure) shows the four different temperature profiles of the 8 μm triangular and the 100 μm thick
393 uniform PDMS-SiO_2-Ag coolers under shaded and unshaded conditions during the peak daytime
394 of Hong Kong (Date: Sep-31-2018). During the daytime, even under the clear sky, 0-1 oktas, it is
395 clear that both coolers without shading were unable to produce a cooling effect. At the peak
396 daytime, both the triangular PDMS cooler and the uniform PDMS cooler without shading was
397 measured with a temperature higher than the ambient air temperature by 5.1 °C and 6.0 °C,
398 respectively. Due to the characteristics of the tropical climate, both coolers, without shading, were
399 unable to deliver cooling performance under the peak solar irradiation as incident solar energy
400 exceeded the radiated thermal energy from the coolers to the atmospheric transparency window.
401 However, even in this poor weather condition for radiative cooling, the triangular structured cooler
402 could maintain a temperature 1 °C below the temperature of the uniform cooler. In order to provide
403 cooling during the peak of Hong Kong's daytime, solar shades, fabricated by aluminum sheet,
404 were installed to shade the coolers during daytime to minimize the incident solar energy delivered
405 to the coolers. With the solar shades partially blocking the incoming sunlight, at the peak daytime,
406 daytime cooling was achieved with the maximum temperature reduction (average temperature

difference between 12:00 – 13:00 (Date: 31-Sep-2018)) of 6.2 °C and 5.1 °C below the ambient for the triangular and uniform, respectively.

Net radiative cooling power measurement of both a uniform 100 µm PDMS-SiO_2-Ag cooler and an 8 µm triangular patterned PDMS-SiO_2-Ag cooler was conducted in a humid climate condition of Hong Kong. Silicon heating mats with a heating capacity of 20 W were attached at the back of both coolers. The cooling power produced by the radiative cooler will be equal to the heating power from the heater when its temperature remains the same as the ambient air temperature. Thus, electrical current flow delivered to the cooling power measurement system was controlled by a feedback loop to maintain the temperature of the cooler equal to the ambient. The net cooling power of these two coolers was estimated by summing up electrical energy consumed by the heater pad in an hourly rate. Fig. 7c presents the collected data for temperature and net cooling power of the uniform 100 µm PDMS-SiO_2-Ag cooler and the 8 µm triangular patterned PDMS-SiO_2-Ag cooler. The peak ambient air temperature during the daytime was measured near 33 °C at 2 pm (08-June-2019), when 19.7 W/m^2 cooling power was recorded for the triangular patterned PDMS cooler, while a net cooling power of 17.9 W/m^2 was obtained from the uniform PDMS cooler. During nighttime operation, the lowest temperature of ambient air was measured at 19 °C (5 am, 08-June-2019) and the triangular patterned PDMS cooler produced 14.3 W/m^2 cooling power, while 13.3 W/m^2 cooling power was recorded for the uniform PDMS cooler. Lower temperature of ambient at night weakened the thermal radiation emitted from both coolers resulting in lower nocturnal cooling power compared to the daytime cooling. In total, both patterned and non-patterned radiative coolers showed weakened cooling performance compared to the outcome

achieved in the clear and dry climatic conditions. Nevertheless, the triangular patterned PDMS cooler showed a 10% enhanced net cooling power than that of the uniform PDMS cooler.

Table 1 summarizes the recent achievements in daytime passive radiative cooling regarding their structural designs, optical properties including solar reflectance and MIR emissivity, and cooling performance. Uniform flat PDMS radiative cooler demonstrated experimentally the highest daytime cooling performance by generating 127 W/m^2 [15]. Optimized TiO_2-SiO_2 alternating multi-layered cooler theoretically predicted a higher net cooling power of 136.6 W/m^2 while its field investigation demonstrated only 14.3 W/m^2 due to the poor sky condition of sub-tropical Hong Kong [13]. The bio-inspired radiative cooler in this work presents the highest cooling performance numerically, showing the net cooling power of 144 W/m^2. However, due to unfavorable sky condition of low atmospheric transparency, its field investigation result shows a net cooling power of 19.7 W/m^2 and temperature reduction of 6.2 °C under direct sunlight. While a majority of the work was conducted under ideal sky conditions, it should be noted that daytime passive radiative cooling is mostly needed in hot sub-tropical or tropical regions. Its cooling performance deteriorates significantly in high humid weather conditions, but by minimizing incoming solar irradiance, daytime cooling effect can be successfully achieved.

5. Conclusion

In conclusion, the bio-inspired thermal selective surface utilizing the unique triangular structure of the Saharan silver ant hair was fabricated by nano-imprinting. Triangular prismatic hair originally functioned to mainly enhance solar reflection, but was unable to meet the required solar reflection for daytime passive cooling. Its application approach in designing a cooler was set to

enhance MIR emissivity by utilizing gradient refractive index change provided by the triangular structure. For the first time, we have demonstrated geometrical modification on a polymeric surface to enhance the emission property. The geometrical details of the triangle and the overall design of the cooler were optimized through the FDTD simulation, proposing a passive radiative cooler design with PDMS triangular arrays at a size characteristic of 8 μm, four times larger than the original hair of the Saharan silver ant, deposited on the silver coated silica wafer. Mathematical analysis on temperature reduction and cooling performance based on optical measurement were conducted to validate the simulation work, proving that the bio-inspired triangular structure can greatly enhance the emissivity within 8-13 μm at the maximum of 0.98, exceeding the cooling performance of existing intricate nanophotonic surfaces. Theoretically, the triangular pattern can enhance the net cooling power to 144 W/m^2 which is the highest value among the developed daytime passive radiative coolers. Also, experimentally, the field investigation on cooling performance of the triangular PDMS cooler was studied in Hong Kong to understand its practicality in a humid weather climate. With the poor atmospheric transparency of Hong Kong's tropical climate, an average atmospheric transmittance within 8-13 μm below 0.5, daytime cooling effect could be achieved using solar shades, and the surface temperature could be sustained at a maximum 6.2 °C below the ambient which corresponds to a net cooling power of 19.7 W/m^2 in a non-vacuumed condition. This investigation delivers a significant meaning by demonstrating the unprecedented daytime passive radiative cooling in a humid climate condition, exceeding the cooling performance of leading coolers which are already available. Overall, applications of triangular prism structure can greatly improve the cooling performance of a plain uniform surface and can be further applied to different surfaces to optimize the desired optical properties. Further modification to the triangular structure can be conducted to maximize the reflection of solar

irradiance to achieve a stronger passive cooling system. Our study facilitates application of passive radiative cooling as a zero-energy input sustainable system to high energy consuming areas such as indoor space cooling [39-41], photovoltaic industry [37, 38], personal thermal managing and regulating system [35, 36].

479 Table 1. Summary of structural design, optical properties and cooling performance of daytime passive radiative coolers.

Authors	Structural Designs	Methodology	Solar Reflectance	MIR Emissivity	Experimental Locations & Conditions	Temperature Reduction (°C)	Cooling Power (W/m^2)
Bao et al. [56]	2 layers of TiO_2, SiO_2, and SiC nanoparticles	Numerical and Field Investigation	0.907	0.90	Shanghai, China Non-vacuum	5	25
Chen et al. [14]	3 layers of 70 nm thick Si_3N_4, 700 µm thick Si, and 150 nm thick Al solar reflector at the back.	Numerical and Field Investigation	0.967	0.56	Stanford, California, USA Vacuum	42	60
Jeong et al. [13]	8 alternating layers of 500 nm thick TiO_2 and 500 nm thick SiO_2 layers with 200 nm thick Ag solar reflector and supported by 750 µm Si layer at the back.	Numerical and Field Investigation	0.942	0.84	Hong Kong, China Non-vacuum	7.2	14.3
Kecebas et al. [54]	Top 9 layers consisting of alternating TiO_2, SiO_2, and Al_2O_3 each 200 nm thick. Lower 4 layers consisting of alternating TiO_2 and SiO_2, each 20 nm thick. 50 nm thick Ag solar reflector at the back.	Numerical	0.960	0.69	N.A.	N.A.	103

Kecebas et al. [54]	Top 9 layers consisting of alternating TiO_2 and SiO_2, each 200 nm thick. Below 4 layers consisting of alternating TiO_2 and SiO_2, each 60 nm thick. 50 nm thick Ag solar reflector at the back.	Numerical	0.965	0.54	N.A.	N.A.	85.8
Kou et al. [15]	3 layers of 100 µm thick PDMS, 500 µm thick SiO_2, and 120 nm thick Ag solar reflector at the back	Numerical and Field Investigation	0.975	0.92	Pasadena, California, USA Non-vacuum	8.2	127
Raman et al. [11]	7 alternating layers of 230 nm thick SiO_2, 485 nm thick HfO_2, 688 nm thick SiO_2, 13 nm thick HfO_2, 73 nm thick SiO_2, 34 nm thick HfO_2, and 54 nm thick SiO_2 with 200 nm thick Ag solar reflector and supported by 750 µm Si layer at the back	Numerical and Field Investigation	0.970	0.65	Stanford, California, USA Non-vacuum	4.9	40.1
Zhai et al. [33]	Micrometer-sized SiO_2 spheres randomly distributed in a matrix material of polymethylpentene (TPX)	Numerical and Field Investigation	0.969	0.93	Cave creek, Arizona, USA Non-vacuum	N.A.	93

This work	3 layers of 8 μm thick triangular prism patterned PDMS, 500 μm thick SiO_2, and 120 nm thick Ag solar reflector at the back	Numerical and Field Investigation	0.975	0.98	Hong Kong, China Non-vacuum	6.2	19.7

480

Conflict of Interest

The authors declare that there is no conflict of interest.

Acknowledgments

The funding for this research is provided by the Hong Kong Research Grant Council via Collaborative Research Fund (CRF) account C6022-16G and General Research Fund (GRF) account 16200518, and also the City University of Hong Kong StartUp Fund via the account code of 9610411. We also acknowledge Nanosystem Fabrication Facility (NFF) of HKUST for the device/system fabrication.

References

[1] S. Catalanotti, V. Cuomo, G. Piro, D. Ruggi, V. Silvestrini, G. Troise, The radiative cooling of selective surfaces, Solar Energy. 17.2 (1975) 83-89. doi:10.1016/0038-092x(75)90062-6.

[2] C.G. Granqvist, A. Hjortsberg, Surfaces for radiative cooling: Silicon monoxide films on aluminum, Applied Physics Letters. 36 (1980) 139–141. doi:10.1063/1.91406.

[3] C.G. Granqvist, A. Hjortsberg, Radiative cooling to low temperatures: General considerations and application to selectively emitting SiO films, Journal of Applied Physics. 52 (1981) 4205–4220. doi:10.1063/1.329270.

[4] A. Harrison, M. Walton, Radiative cooling of TiO2 white paint, Solar Energy. 20 (1978) 185–188. doi:10.1016/0038-092x(78)90195-0.

[5] P. Berdahl, M. Martin, F. Sakkal, Thermal performance of radiative cooling panels, International Journal of Heat and Mass Transfer. 26 (1983) 871–880. doi:10.1016/s0017-9310(83)80111-2.

[6] P. Berdahl, Radiative cooling with MgO and/or LiF layers, Applied Optics. 23 (1984) 370-372. doi:10.1364/ao.23.000370.

[7] T.M. Nilsson, G.A. Niklasson, C.G. Granqvist, A solar reflecting material for radiative cooling applications: ZnS pigmented polyethylene, Solar Energy Materials and Solar Cells. 28 (1992) 175–193. doi:10.1016/0927-0248(92)90010-m.

[8] T.M. Nilsson, G.A. Niklasson, Radiative cooling during the day: simulations and experiments on pigmented polyethylene cover foils, Solar Energy Materials and Solar Cells. 37 (1995) 93–118. doi:10.1016/0927-0248(94)00200-2.

[9] P. Berdahl, Comments on radiative cooling efficiency of white pigmented paints, Solar Energy. 54 (1995) 203. doi:10.1016/0038-092x(95)90031-a.

[10] C.N. Suryawanshi, C.-T. Lin, Radiative Cooling: Lattice Quantization and Surface Emissivity in Thin Coatings, ACS Applied Materials & Interfaces. 1 (2009) 1334–1338. doi:10.1021/am900200r.

[11] A.P. Raman, M.A. Anoma, L. Zhu, E. Rephaeli, S. Fan, Passive radiative cooling below ambient air temperature under direct sunlight, Nature. 515 (2014) 540–544. doi:10.1038/nature13883.

[12] C. Tso, K. Chan, C.Y. Chao, A field investigation of passive radiative cooling under Hong Kong's climate, Renewable Energy. 106 (2017) 52–61. doi:10.1016/j.renene.2017.01.01.

[13] S.Y. Jeong, C.Y. Tso, J. Ha, Y.M. Wong, C.Y. Chao, B. Huang, et al., Field investigation of a photonic multi-layered TiO2 passive radiative cooler in sub-tropical climate, Renewable Energy. 146 (2020) 44–55. doi:10.1016/j.renene.2019.06.119.

[14] Z. Chen, L. Zhu, A. Raman, S. Fan, Radiative cooling to deep sub-freezing temperatures through a 24-h day–night cycle, Nature Communications. 7 (2016). doi:10.1038/ncomms13729.

[15] J.-L. Kou, Z. Jurado, Z. Chen, S. Fan, A.J. Minnich, Daytime Radiative Cooling Using Near-Black Infrared Emitters, ACS Photonics. 4 (2017) 626–630. doi:10.1021/acsphotonics.6b00991.

[16] S.-Y. Lin, J.G. Fleming, E. Chow, J. Bur, K.K. Choi, A. Goldberg, Enhancement and suppression of thermal emission by a three-dimensional photonic crystal, Physical Review B. 62 (2000). doi:10.1103/physrevb.62.r2243.

[17] A. Narayanaswamy, G. Chen, Thermal emission control with one-dimensional metallodielectric photonic crystals, Physical Review B. 70 (2004). doi:10.1103/physrevb.70.125101.

[18] I. Celanovic, D. Perreault, J. Kassakian, Resonant-cavity enhanced thermal emission, Physical Review B. 72 (2005). doi:10.1103/physrevb.72.075127.

[19] E. Rephaeli, S. Fan, Absorber and emitter for solar thermo-photovoltaic systems to achieve efficiency exceeding the Shockley-Queisser limit, Optics Express. 17 (2009) 15145-15159. doi:10.1364/oe.17.015145.

[20] J.L. Gall, M. Olivier, J.-J. Greffet, Experimental and theoretical study of reflection and coherent thermal emissionby a SiC grating supporting a surface-phonon polariton, Physical Review B. 55 (1997) 10105–10114. doi:10.1103/physrevb.55.10105.

[21] J.B. Pendry, Radiative exchange of heat between nanostructures, Journal of Physics: Condensed Matter. 11 (1999) 6621–6633. doi:10.1088/0953-8984/11/35/301.

[22] C. Luo, A. Narayanaswamy, G. Chen, J.D. Joannopoulos, Thermal Radiation from Photonic Crystals: A Direct Calculation, Physical Review Letters. 93 (2004). doi:10.1103/physrevlett.93.213905.

[23] D.L.C. Chan, M. Soljačić, J.D. Joannopoulos, Thermal emission and design in one-dimensional periodic metallic photonic crystal slabs, Physical Review E. 74 (2006). doi:10.1103/physreve.74.016609.

[24] D.L.C. Chan, M. Soljačić, J.D. Joannopoulos, Thermal emission and design in 2D-periodic metallic photonic crystal slabs, Optics Express. 14 (2006) 8785-8796. doi:10.1364/oe.14.008785.

[25] J.G. Fleming, S.Y. Lin, I. El-Kady, R. Biswas, K.M. Ho, All-metallic three-dimensional photonic crystals with a large infrared bandgap, Nature. 417 (2002) 52–55. doi:10.1038/417052a.

[26] E. Rephaeli, S. Fan, Tungsten black absorber for solar light with wide angular operation range, Applied Physics Letters. 92 (2008) 211107. doi:10.1063/1.2936997.

[27] K.A. Arpin, M.D. Losego, P.V. Braun, Electrodeposited 3D Tungsten Photonic Crystals with Enhanced Thermal Stability, Chemistry of Materials. 23 (2011) 4783–4788. doi:10.1021/cm2019789.

[28] M. Wang, C. Hu, M. Pu, C. Huang, Z. Zhao, Q. Feng, et al., Truncated spherical voids for nearly omnidirectional optical absorption, Optics Express. 19 (2011) 20642-20649. doi:10.1364/oe.19.020642.

[29] S. Zhang, Y. Li, G. Feng, B. Zhu, S. Xiao, L. Zhou, et al., Strong infrared absorber: surface-microstructured Au film replicated from black silicon, Optics Express. 19 (2011) 20462-20467. doi:10.1364/oe.19.020462.

570 [30] M.M. Hossain, B. Jia, M. Gu, Metamaterials: A Metamaterial Emitter for Highly Efficient
571 Radiative Cooling (Advanced Optical Materials 8/2015), Advanced Optical Materials. 3
572 (2015) 980–980. doi:10.1002/adom.201570046.
573 [31] C. Zou, G. Ren, M.M. Hossain, S. Nirantar, W. Withayachumnankul, T. Ahmed, et al., Metal-
574 Loaded Dielectric Resonator Metasurfaces for Radiative Cooling, Advanced Optical
575 Materials. 5 (2017) 1700460. doi:10.1002/adom.201700460.
576 [32] K. Hwang, Y.-S. Jung, Y.-J. Heo, F.H. Scholes, S.E. Watkins, J. Subbiah, et al., Toward Large
577 Scale Roll-to-Roll Production of Fully Printed Perovskite Solar Cells, Advanced Materials.
578 27 (2015) 1241–1247. doi:10.1002/adma.201404598.
579 [33] Y. Zhai, Y. Ma, S.N. David, D. Zhao, R. Lou, G. Tan, et al., Scalable-manufactured
580 randomized glass-polymer hybrid metamaterial for daytime radiative cooling, Science. 355
581 (2017) 1062–1066. doi:10.1126/science.aai7899.
582 [34] A.R. Gentle, G.B. Smith, Radiative Heat Pumping from the Earth Using Surface Phonon
583 Resonant Nanoparticles, Nano Letters. 10 (2010) 373–379. doi:10.1021/nl903271d.
584 [35] P.-C. Hsu, X. Liu, C. Liu, X. Xie, H.R. Lee, A.J. Welch, et al., Personal Thermal Management
585 by Metallic Nanowire-Coated Textile, Nano Letters. 15 (2014) 365–371.
586 doi:10.1021/nl5036572.
587 [36] J.K. Tong, X. Huang, S.V. Boriskina, J. Loomis, Y. Xu, G. Chen, Infrared-Transparent
588 Visible-Opaque Fabrics for Wearable Personal Thermal Management, ACS Photonics. 2
589 (2015) 769–778. doi:10.1021/acsphotonics.5b00140.
590 [37] L. Zhu, A. Raman, K.X. Wang, M.A. Anoma, S. Fan, Radiative cooling of solar cells, Optica.
591 1 (2014) 32-38. doi:10.1364/optica.1.000032.

592 [38] W. Li, Y. Shi, K. Chen, L. Zhu, S. Fan, Passive cooling of solar cells with a comprehensive
593 photonic approach, 2017 IEEE 60th International Midwest Symposium on Circuits and
594 Systems (MWSCAS). (2017). doi:10.1109/mwscas.2017.8053056.
595 [39] E.A. Goldstein, A.P. Raman, S. Fan, Sub-ambient non-evaporative fluid cooling with the sky,
596 Nature Energy. 2 (2017). doi:10.1038/nenergy.2017.143.
597 [40] W. Wang, N. Fernandez, S. Katipamula, K. Alvine, Performance assessment of a photonic
598 radiative cooling system for office buildings, Renewable Energy. 118 (2018) 265–277.
599 doi:10.1016/j.renene.2017.10.062.
600 [41] S.Y. Jeong, C.Y. Tso, M. Zouagui, Y.M. Wong, C.Y.H. Chao, A numerical study of daytime
601 passive radiative coolers for space cooling in buildings, Building Simulation. 11 (2018) 1011–
602 1028. doi:10.1007/s12273-018-0474-4.
603 [42] C. Paquet, E. Kumacheva, Nanostructured polymers for photonics, Materials Today. 11 (2008)
604 48–56. doi:10.1016/s1369-7021(08)70056-7.
605 [43] R. Wehner, A.C. Marsh, S. Wehner, Desert ants on a thermal tightrope, Nature. 357 (1992)
606 586–587. doi:10.1038/357586a0.
607 [44] N.N. Shi, C.-C. Tsai, F. Camino, G.D. Bernard, N. Yu, R. Wehner, Keeping cool: Enhanced
608 optical reflection and radiative heat dissipation in Saharan silver ants, Science. 349 (2015)
609 298–301. doi:10.1126/science.aab3564.
610 [45] Q. Willot, P. Simonis, J.-P. Vigneron, S. Aron, Total Internal Reflection Accounts for the
611 Bright Color of the Saharan Silver Ant, Plos One. 11 (2016).
612 doi:10.1371/journal.pone.0152325.
613 [46] C.F. Bohren, D.R. Huffman, Absorption and scattering of light by small particles, Wiley-
614 VCH, Weinheim, 2009.

[47] A. Srinivasan, B. Czapla, J. Mayo, A. Narayanaswamy, Infrared dielectric function of polydimethylsiloxane and selective emission behavior, Applied Physics Letters. 109 (2016) 061905. doi:10.1063/1.4961051.

[48] O. Tabata, R. Asahi, H. Funabashi, K. Shimaoka, S. Sugiyama, Anisotropic etching of silicon in TMAH solutions, Sensors and Actuators A: Physical. 34 (1992) 51–57. doi:10.1016/0924-4247(92)80139-t.

[49] A. Berk, G.P. Anderson, P.K. Acharya, L.S. Bernstein, L. Muratov, J. Lee, et al., MODTRAN5: 2006 update, Algorithms and Technologies for Multispectral, Hyperspectral, and Ultraspectral Imagery XII. (2006). doi:10.1117/12.665077.

[50] S.D. Lord, A new software tool for computing earth's atmospheric transmission of near- and far-infrared radiation, Ames Research Center, Moffett Field, CA, 1992.

[51] C. Gueymard, D. Myers, K. Emery, Proposed reference irradiance spectra for solar energy systems testing, Solar Energy. 73 (2002) 443-467. Doi:10.1016/s0038-092x(03)00005-7

[52] Tables for Reference Solar Spectral Irradiances: Direct Normal and Hemispherical on 37 Tilted Surface, (n.d.). doi:10.1520/g0173.

[53] P. Yang, C. Chen, Z.M. Zhang, A dual-layer structure with record-high solar reflectance for daytime radiative cooling, Solar Energy. 169 (2018) 316–324. doi:10.1016/j.solener.2018.04.031.

[54] M.A. Kecebas, M.P. Menguc, A. Kosar, K. Sendur, Passive radiative cooling design with broadband optical thin-film filters, Journal of Quantitative Spectroscopy and Radiative Transfer. 198 (2017) 179–186. doi:10.1016/j.jqsrt.2017.03.046.

[55] Z. Huang, X. Ruan, Nanoparticle embedded double-layer coating for daytime radiative cooling, International Journal of Heat and Mass Transfer. 104 (2017) 890–896. doi:10.1016/j.ijheatmasstransfer.2016.08.009.

[56] H. Bao, C. Yan, B. Wang, X. Fang, C. Zhao, X. Ruan, Double-layer nanoparticle-based coatings for efficient terrestrial radiative cooling, Solar Energy Materials and Solar Cells. 168 (2017) 78–84. doi:10.1016/j.solmat.2017.04.020.

Figure Captions

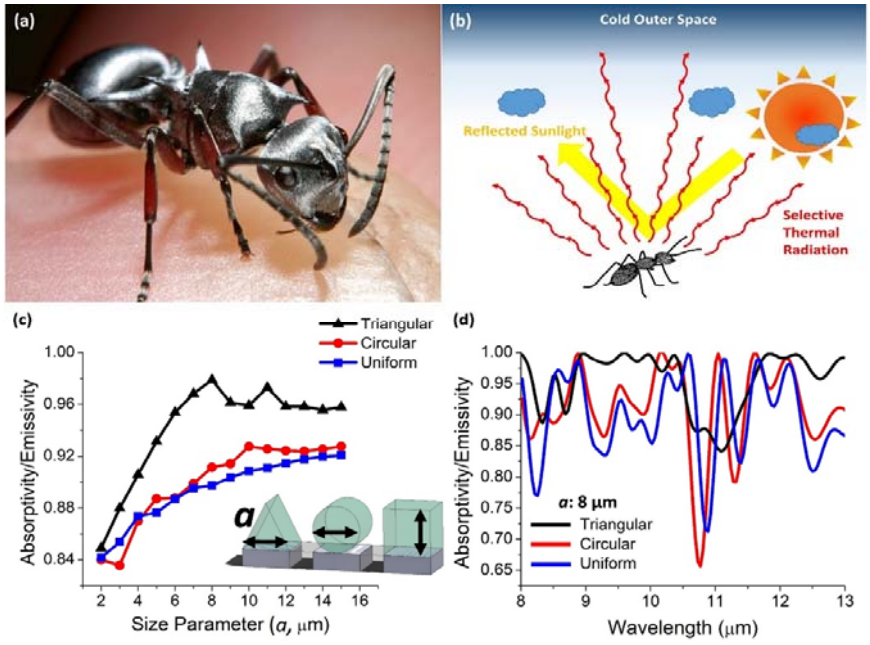

Fig. 1. (a) Photograph of Saharan silver ant, *Cataglyphis bombycina* (b) A schematic diagram of thermoregulatory effect discovered in the Saharan silver ant (c) FDTD simulation result for averaged MIR emissivity (8-13 μm) of three different geometrical configurations (triangular prism arrays (black solid line), circular rod arrays (red solid line), and uniform flat layer (blue solid line)) along with characteristic length of 2-15 μm (d) FDTD simulation result for MIR emission spectrum (8-13 μm) of emitters with triangular prism arrays (black solid line), circular rod arrays (red solid line), and uniform flat layer (blue solid line) at a constant characteristic length of 8 μm

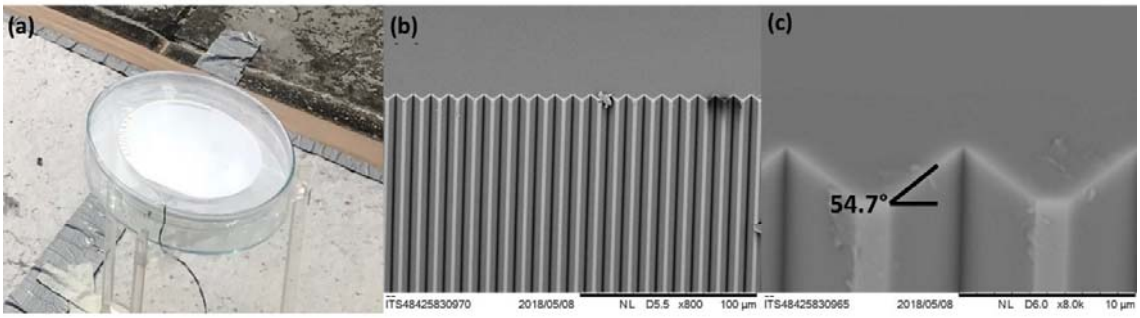

Fig. 2. (a) A fabricated 4-inch wafer size 8 µm characteristic length triangular PDMS-SiO_2-Ag daytime passive radiative cooler under direct sunlight. (b) SEM image of the fabricated silicon mold with 8 µm characteristic length triangular arrays with a scale bar at 100 µm. (c) SEM image of the fabricated silicon mold with 8 µm characteristic length triangular arrays with a scale bar at 10 µm.

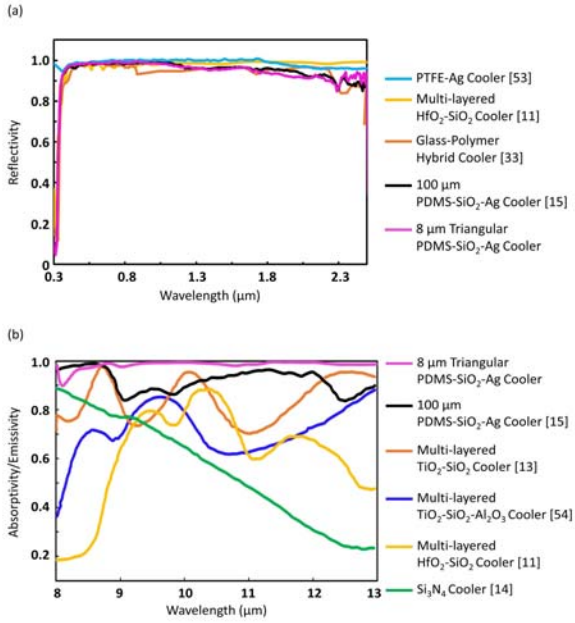

Fig. 3. (a) Measured full emission spectrum of the uniform 100 μm thick PDMS-SiO_2-Ag (black solid line) and the patterned PDMS-SiO_2-Ag with triangular prism array of a size parameter at 8 μm (pink solid line) in the wavelength range of 0.25-25 μm. (b) Measured emissivity of the uniform 100 μm thick PDMS-SiO_2-Ag (black solid line), the patterned PDMS-SiO_2-Ag with triangular prism array of a size parameter at 8 μm (pink solid line), a size parameter at 9 μm (blue solid line), a size parameter at 10 μm (green solid line) in the wavelength range of 0.25-2.5 μm. The AM 1.5 solar spectrum (red solid line). (c) Measured emissivity of the uniform 100 μm thick PDMS-SiO_2-Ag (black solid line), the patterned PDMS-SiO_2-Ag with triangular prism arrays of a size parameter at 8 μm (pink solid line), a size parameter at 9 μm (blue solid line), a size parameter at 10 μm (green solid line) in the wavelength range of 8-13 μm.

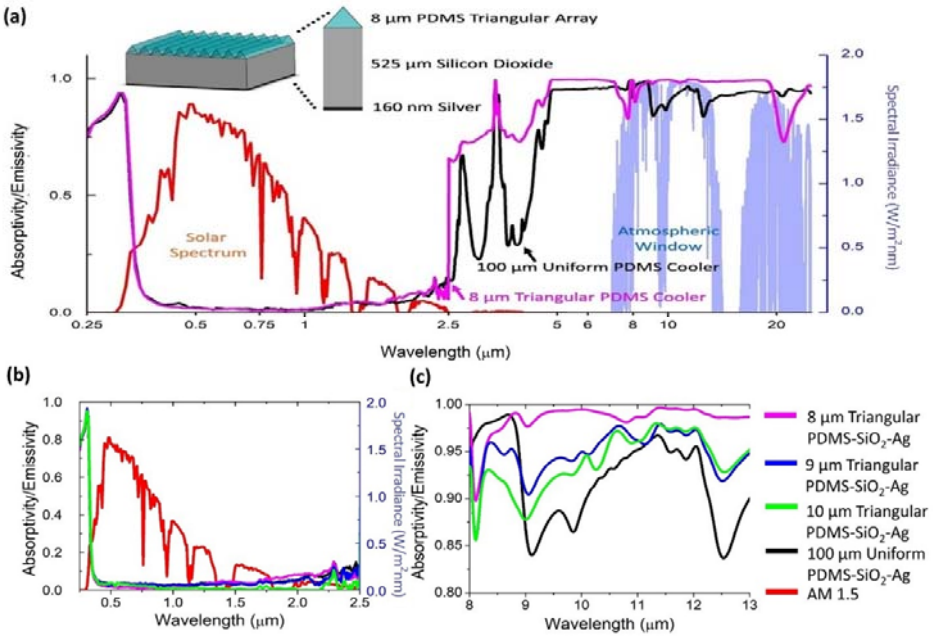

Fig. 4. (a) Reflectivity spectrum within 0.3-2.5 µm of PTFE-Ag cooler [53] (light blue solid line), HfO_2-SiO_2 alternating multi-layered radiative cooler [11] (yellow solid line), glass-polymer hybrid cooler [33] (orange solid line), 100 µm uniform PDMS polymer based radiative cooler [15] (black solid line), and 8 µm triangular PDMS polymer based radiative cooler (pink solid line, this work) (b) Emission spectrum within 8-13 µm of 8 µm triangular PDMS polymer based radiative cooler (pink solid line, this work), 100 µm uniform PDMS polymer based radiative cooler [15] (black solid line), TiO_2-SiO_2 alternating multi-layered radiative cooler [13] (orange solid line), TiO_2-SiO_2-Al_2O_3 alternating multi-layered radiative cooler [54] (blue solid line), HfO_2-SiO_2 alternating multi-layered radiative cooler [11] (yellow solid line), and Si_3N_4 based radiative cooler [14] (green solid line).

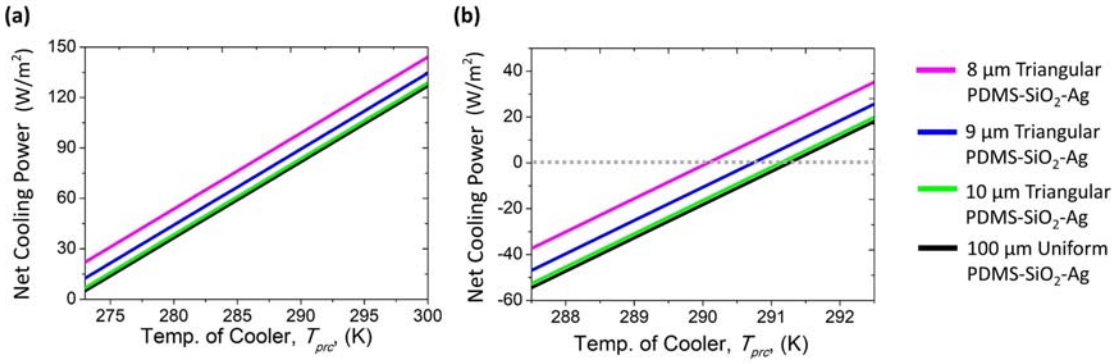

Fig. 5. (a) Numerically estimated cooling power of the uniform 100 μm thick PDMS-SiO_2-Ag (black solid line), the patterned PDMS-SiO_2-Ag with triangular prism arrays of a size parameter at 8 μm (pink solid line), a size parameter at 9 μm (blue solid line), a size parameter at 10 μm (green solid line) with changing cooler temperature at a heat gain codition of h_{con} = 0 W/(m^2K). (b) Numerically estimated cooling power of the uniform 100 μm thick PDMS-silica-mirror (black solid line), the patterned PDMS-SiO_2-Ag with triangular prism arrays of a size parameter at 8 μm (pink solid line), a size parameter at 9 μm (blue solid line), a size parameter at 10 μm (green solid line) with changing cooler temperature at a heat gain condition of h_{con}= 10 W/(m^2K).

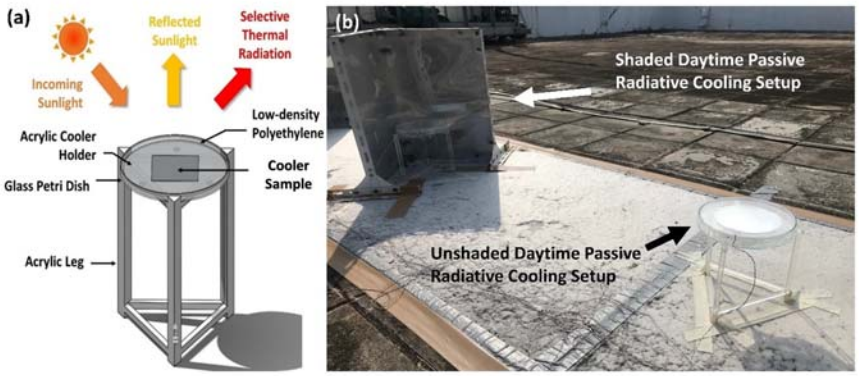

60

61

62 Fig. 6. (a) A schematic diagram of experimental setup for daytime passive radiative cooling (b)

63 Experimental setups for both shaded and unshaded daytime passive radiative cooling.

64

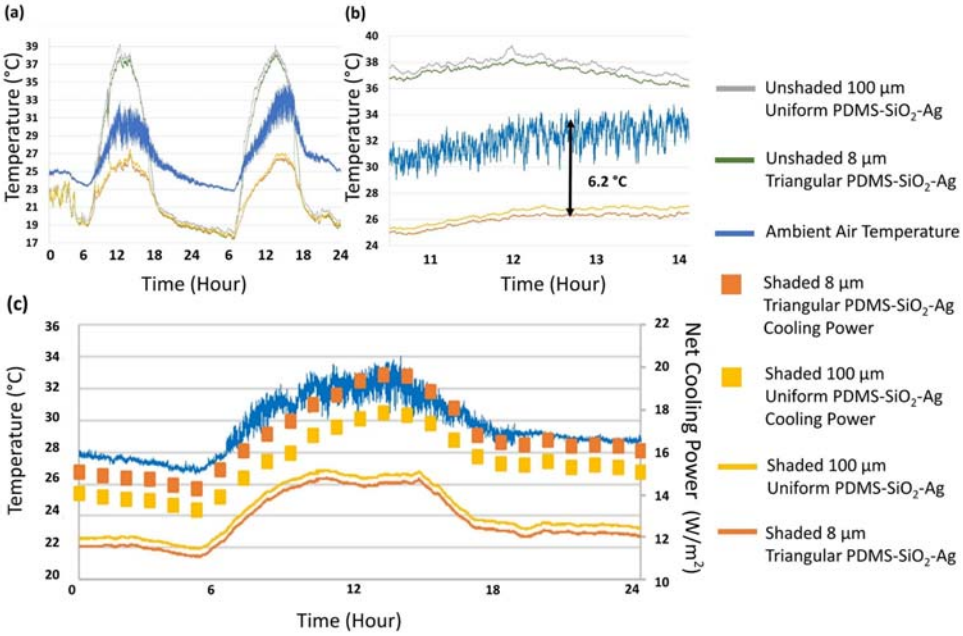

Fig. 7. (a) Temperature profile of the unshaded uniform 100 µm thick PDMS-SiO_2-Ag (grey solid line), the unshaded 8 µm triangle PDMS-SiO_2-Ag (green solid line), and the temperature of ambient (blue solid line), the shaded uniform 100 µm thick PDMS-SiO_2-Ag (yellow solid line), the shaded 8 µm PDMS-SiO_2-Ag (orange), through a 48 hrs cycle (Date: 30-Sep-2018 to 31-Sep-2018). The average daytime relative humidity was 87 % and 0-1 oktas sky condition was observed. The average global solar intensity was measured to be 1010 W/m^2 at peak daytime (11:00 am to 13:00 pm). (b) Zoom-in of the temperature profile (Date: 31-Sep-2018) with the device under direct solar irradiation. The shaded 8 µm triangle PDMS-SiO_2-Ag cooler (orange solid line) achieved a temperature 6.2 °C below the temperature of ambient. (c) Net cooling power (square box) and temperature (line) profiles of the shaded 100 µm uniform PDMS-SiO_2-Ag cooler (yellow) and the shaded 8 µm triangular patterned PDMS-SiO_2-Ag cooler (orange) at the ambient air temperature (blue) during a 24-hr cycle (Date: 08-June-2019). The average relative humidity during the daytime and nighttime was 85 % and 65 %, respectively. 0-1 oktas sky condition was observed. The average global solar

intensity was measured at 1020 W/m^2 during the peak daytime (from 12:00 pm to 2:00 pm).

Supplementary Materials

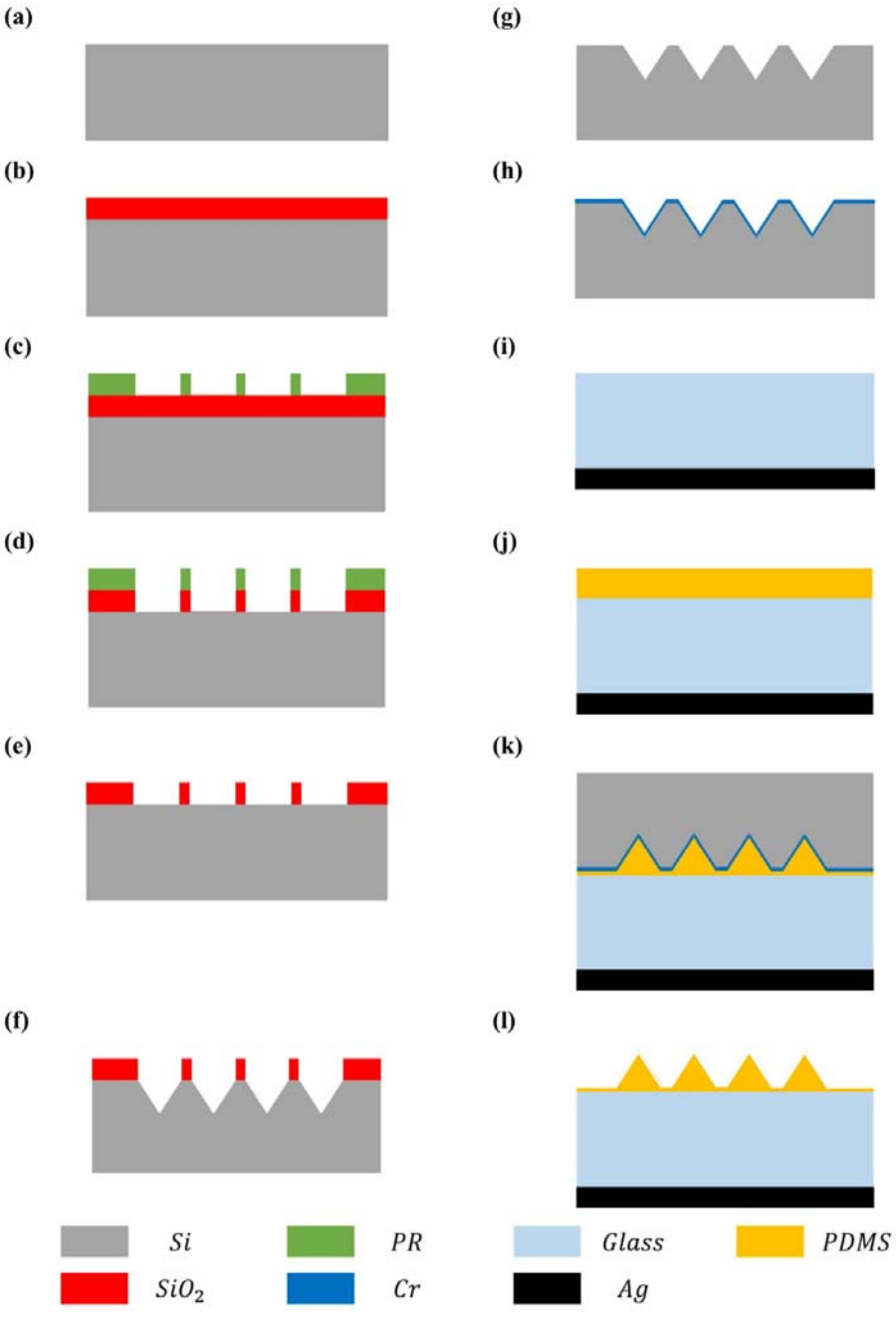

Fig. S1. Fabrication process flow of the bio-inspired passive radiative cooler. (a) Preparation of a 525 μm thick P-type 4-inch silicon wafer cleaned by Piranha and hydrofluoric acid solution. (b) Thermal oxidation of the silicon wafer for 60 nm. (c) Photo-lithography of the pattern on the silicon wafer. (d) AOE process to etch the thermal oxide layer for 30 s. (e) Photo resist layer strip off process. (f) Silicon wet etching process with TMAH solution (g) BOE

process to remove the remaining thermal oxide layer. (h) Sputter 160 nm thickness chromium on the surface of the mold. (i) Sputter 160 nm Silver at the back of the silicon dioxide substrate. (j) Spin-coat 20 µm PDMS on the silicon dioxide substrate. (k) Nano-imprint process (l) Removal of the mold after baking.